Research Article
Hepatic and Biliary Cancer

JOURNAL OF HEPATOLOGY

A myeloid immunosuppressive phenotype defines primary refractoriness to atezolizumab plus bevacizumab in hepatocellular carcinoma

Authors

Pasquale Lombardi, Erik Ramon-Gil, Rabial Q. Raja, …, Hong Jae Chon, Jack Leslie, David J. Pinato

Correspondence

minidoctor@cha.ac.kr (H.J. Chon), Jack.Leslie@newcastle.ac.uk (J. Leslie), david.pinato@imperial.ac.uk (D.J. Pinato).

Graphical abstract

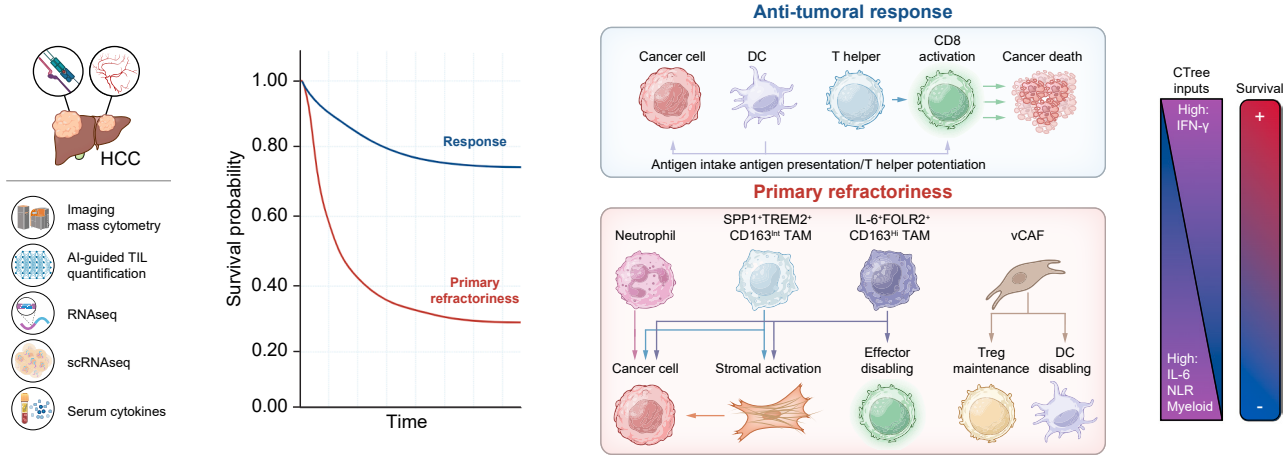

Highlights

- 45% of patients with HCC show primary refractoriness to atezolizumab-bevacizumab.
- PRef confers a significantly higher mortality risk across clinical settings.
- PRef is characterised by a myeloid immunosuppressive phenotype with T-cell depletion.
- Systemic NLR mirrors intratumoral immunosuppressive myeloid infiltration.
- A CTree model integrating IFN-γ and NLR defined a high-risk subgroup with a 74% probability of PRef.

Impact and implications

Atezolizumab plus bevacizumab represents the standard first-line treatment for unresectable hepatocellular carcinoma, yet the biological basis of early treatment failure remains poorly understood. In this multi-cohort translational study, we show that approximately 40% of patients exhibit primary refractoriness according to SITC criteria – clinically validated here for the first time in hepatocellular carcinoma – and identify a distinct immuno-molecular profile of primary refractory tumours characterised by IFN-γ pathway repression, unfavourable myeloid polarisation, and a distinct spatial immune architecture. These findings provide a biological framework that may inform the design of biomarker-stratified trials and rational combination strategies to overcome primary resistance to first-line immunotherapy.

https://doi.org/10.1016/j.jhep.2026.05.018

Research Article
Hepatic and Biliary Cancer

JOURNAL
OF HEPATOLOGY

A myeloid immunosuppressive phenotype defines primary refractoriness to atezolizumab plus bevacizumab in hepatocellular carcinoma

Pasquale Lombardi[1,2,†], **Erik Ramon-Gil**[3,†], Rabial Q. Raja[3], Leonardo Brunetti[1], Giulia Francesca Manfredi[1,4], Zhongguo Zhou[1], George Merces[5], Sarah Cappuyns[1,6], Claudia Angela Maria Fulgenzi[1], Antonio D'Alessio[1], Aria Torkpour[1], Ciro Celsa[1,7], Bernardo Stefanini[1,8], Hannah Yang[9], Fionnuala Crowley[10], Thomas U. Marron[10], Anwaar Saeed[11], Matthias Pinter[12], Bernhard Scheiner[12], Yi-Hsiang Huang[13,14,15], Pei-Chang Lee[1,14], Naoshi Nishida[16], Ryan Po-Ting Lin[17], Andrea Dalbeni[18], Caterina Vivaldi[19], Gianluca Masi[19], Natascha Rohlen[20], Johann von Felden[21], Ahmed Kaseb[22], Peter R. Galle[23], Masatoshi Kudo[16], Wei-Fan Hsu[24], Lorenza Rimassa[25,26], Alessandro Parisi[27], Robin Kate Kelley[28], Hidenori Toyoda[29], Mario Pirisi[4], Falah Jabar[1,30], Mehrdad Rakaee[30,31,32,33], Giuseppe Cabibbo[7,34], Calogero Cammà[7], Fabio Piscaglia[8,35], Sohyun Hwang[36], Dong Jun Shin[37], Michael Li[38], Jeroen Dekervel[6], Nadia Guerra[39], Tim Meyer[40], Helen L. Reeves[3,41,42], Bertram Bengsch[20], Gennaro Daniele[2], Derek A. Mann[3], Hong Jae Chon[9,*,#], Jack Leslie[3,42,*,#], David J. Pinato[1,4,*,#]

Journal of Hepatology **2026**. vol. ■ | 1–13

Background & Aims: Despite improved outcomes with atezolizumab plus bevacizumab (A+B) in hepatocellular carcinoma, primary refractoriness (PRef), characterised by early progression or short-lived disease stabilisation following treatment, remains a significant challenge.

Methods: We analysed 1,296 patients with hepatocellular carcinoma treated with frontline A+B (AB-real) and validated findings in 645 trial participants recruited to IMbrave150 and GO30140. PRef was defined by SITC (Society for the Immunotherapy of Cancer) criteria. We performed a multi-parametric analysis of pre-treatment tumour tissue, including machine learning-based quantification of tumour-infiltrating lymphocytes, imaging mass cytometry and RNA sequencing (RNA-seq) to evaluate differences in the tumour microenvironment (TME) of patients with PRef *vs.* responders. Two independent cohorts were further used to refine the TME characterisation through single-cell RNA-seq (n = 20) and imaging mass cytometry (n = 16). We employed conditional inference tree analyses to provide a hierarchical organisation of PRef determinants.

Results: Among 677 AB-real patients and 378 trial participants evaluable by SITC criteria, PRef was associated with inferior median overall survival compared to response (AB-real: 7.3 *vs.* 31.5 months, p <0.001; Trials: 10.8 *vs.* not reached, p <0.001). Patients with PRef exhibited higher baseline systemic inflammation (neutrophil-to-lymphocyte ratio [NLR] ≥3), a distinctly immunosuppressive TME enriched in CD163+ tumour-associated macrophages and vascular cancer-associated fibroblasts, a higher Treg/Teff cell ratio, and pro-tumour supportive cellular interactions. RNA-seq of tumour tissue confirmed lower intrinsic immunogenicity in PRef samples with elevated myeloid infiltration. Conditional inference tree analysis identified IFN-γ signature downregulation combined with NLR ≥3 as the strongest contributor of PRef.

Conclusions: PRef to A+B identifies a distinct biological entity characterised by unopposed systemic inflammation, myeloid infiltration, and T-cell depletion. Targeting myeloid-mediated immunosuppression, particularly in patients with low IFN-γ signature expression and elevated NLR might enhance responsiveness to A+B.

Introduction

The prognostic outlook for patients with unresectable advanced hepatocellular carcinoma (HCC) has improved remarkably in recent years due to the introduction of immune checkpoint inhibitors (ICIs), which have shifted the expected median overall survival (OS) from approximately 10-13 months with sorafenib to up to 19.2 months with the combination of atezolizumab plus bevacizumab (A+B), the first

* Corresponding authors. Addresses: Department of Surgery and Cancer, Imperial College London Hammersmith Campus, Du Cane Road, W12 0HS, London, UK, Tel.: +44 0207 5942799 (D.J. Pinato), or The Newcastle University Centre for Cancer, Newcastle University, Newcastle Upon Tyne, UK, Tel.: +44 01912086890 (J. Leslie), or Department of Medical Oncology, CHA Bundang Medical Center, CHA University School of Medicine, 59 Yatap-ro, Bundang-gu, Seongnam 13496, Korea, Tel.: +82 31 780 7590 (H.J. Chon).
E-mail addresses: david.pinato@imperial.ac.uk (D.J. Pinato), Jack.Leslie@newcastle.ac.uk (J. Leslie), minidoctor@cha.ac.kr (H.J. Chon).
† Co-first authors
# Co-last senior contributors
https://doi.org/10.1016/j.jhep.2026.05.018

immunotherapy combination to be introduced in clinical practice.[1–3]

While survival improvements associated with PD-1/PD-L1 inhibitor-containing combinations have been amply validated across several studies evaluating combinations with VEGF inhibitors, tyrosine kinase inhibitors (TKIs), and CTLA-4 inhibitors,[4,5] the proportion of patients who achieve a measurable response remains confined to a minority ranging from 20% to 36%.[4]

While an objective response is not required to derive survival benefit from all ICI regimens,[2,6] disease progression on immunotherapy remains invariably associated with poor prognosis in HCC.[2,6–8] Resistance may be either adaptive, occurring after an initial clinical benefit, or primary refractoriness (PRef), characterised by early disease progression without a prior response. In solid tumours, PRef reflects low intrinsic immunogenicity of the tumour, due to impaired antigen presentation, low neoantigen load, or an immunosuppressive microenvironment – features that are biologically distinct from adaptive resistance and associated with worse outcomes.[9] Acknowledging the fundamental differences in the immunobiology underlying the various patterns of resistance, the Society for Immunotherapy of Cancer (SITC) has developed consensus recommendations for defining resistance to ICI based on observed responses to treatment, providing a standardised framework to reproducibly identify PRef tumours in the clinic.[10]

Despite their clinical utility, these criteria have not been validated in HCC, a disease where prognosis is not only dictated by tumour progression but uniquely influenced by concomitant liver dysfunction.[11] In addition, while predictors of response to A+B have been explored, the biological and clinical features of patients with PRef remain poorly characterised.[12,13]

In this study, we aimed to characterise the clinical course of patients with HCC exhibiting PRef to A+B. Leveraging clinical data and pre-treatment tumour samples from a large observational cohort and two landmark clinical trials in unresectable/advanced HCC, we validated SITC-defined PRef and explored its underlying biological determinants to identify prognostic factors and potential therapeutic targets for overcoming primary resistance.

Patients and methods

Study design and clinical outcomes

Patient disposition across studied cohorts is summarised in Fig. 1. The study design and methods for AB-real,[7] GO30140 (NCT02715531),[14] IMbrave150 (NCT03434379)[15] and Cohort 4[16] have been previously described. Cohort 5 consisted of an independent series of 16 patients with HCC treated with frontline A+B, whose pre-treatment formalin-fixed paraffin-embedded (FFPE) tissue was used for imaging mass cytometry (IMC) validation of Cohort 1 findings.

The SITC consensus criteria were applied to identify primary resistance or refractoriness: PRef was defined as the achievement of progressive disease or stable disease lasting <6 months as best overall response to ICI in all cohorts.[10] Responders were defined as patients who achieved a complete response, a partial response or stable disease lasting ≥6 months as best overall response to ICI in all cohorts. Radiological response to treatment was assessed according to RECIST criteria v1.1.

Patients who discontinued treatment before 6 months due to toxicity, clinical deterioration, or other non-progression reasons without documented radiological progression were excluded to ensure that PRef captured true primary resistance rather than treatment intolerance. Details on study design, patient assessments and response outcomes are described in the supplementary methods.

Machine-learning approach for tumour-infiltrating lymphocyte identification and quantification

We applied a supervised machine learning algorithm to 37 and 184 H&E-stained slides from Cohort 1 and Cohorts 2–3, respectively. The algorithm was developed using QuPath (v0.5.0) and implemented following a previously described procedure, with minor modifications (Fig. 1).[17] A detailed description of model development, training and quality verification can be found in the supplementary methods.

Imaging mass cytometry

FFPE pre-treatment biopsies (n = 43 from Cohort 1 and n = 16 from Cohort 5) were stained with a panel of metal-conjugated antibodies previously validated by immunohistochemistry and analysed using IMC. A total of 441 and 121 regions of interest were acquired using the Hyperion system in Cohort 1 and 5, respectively. Image segmentation and single-cell identification were performed using the OPTIMAL pipeline, and cells were clustered into phenotypes via the FlowSOM algorithm (details in the supplementary methods and Tables S1 and S2). Spatial cell–cell interaction analysis was conducted as described in the supplementary methods.

Serum cytokine quantification

Peripheral blood samples were obtained immediately before the first administration of A+B in 182 patients of Cohort 1 (Fig. 1). A detailed description of the procedure can be found in the supplementary methods.

Single-cell RNA sequencing

Single-cell RNA sequencing (scRNA-seq) data from Cohort 4 were analysed using the Seurat R package (version 5.3.0). Quality control procedures were applied to remove low-quality cells based on total unique molecular identifier counts, number of detected genes and mitochondrial gene content, together with the exclusion of genes detected in fewer than three cells. Doublets were identified using scDblFinder and removed prior to downstream analyses. Gene expression data were normalized using Seurat's NormalizeData function, and highly variable genes were identified using the variance-stabilizing transformation method. Dimensionality reduction was performed using principal component analysis followed by unsupervised clustering according to the standard Seurat workflow.

Major cell populations were annotated based on the expression of canonical lineage markers. As the focus of this study was the immune tumour microenvironment (TME), malignant epithelial cells were excluded from downstream analyses. To identify finer cellular subtypes, immune cell populations were subsequently re-clustered after batch correction using the Harmony

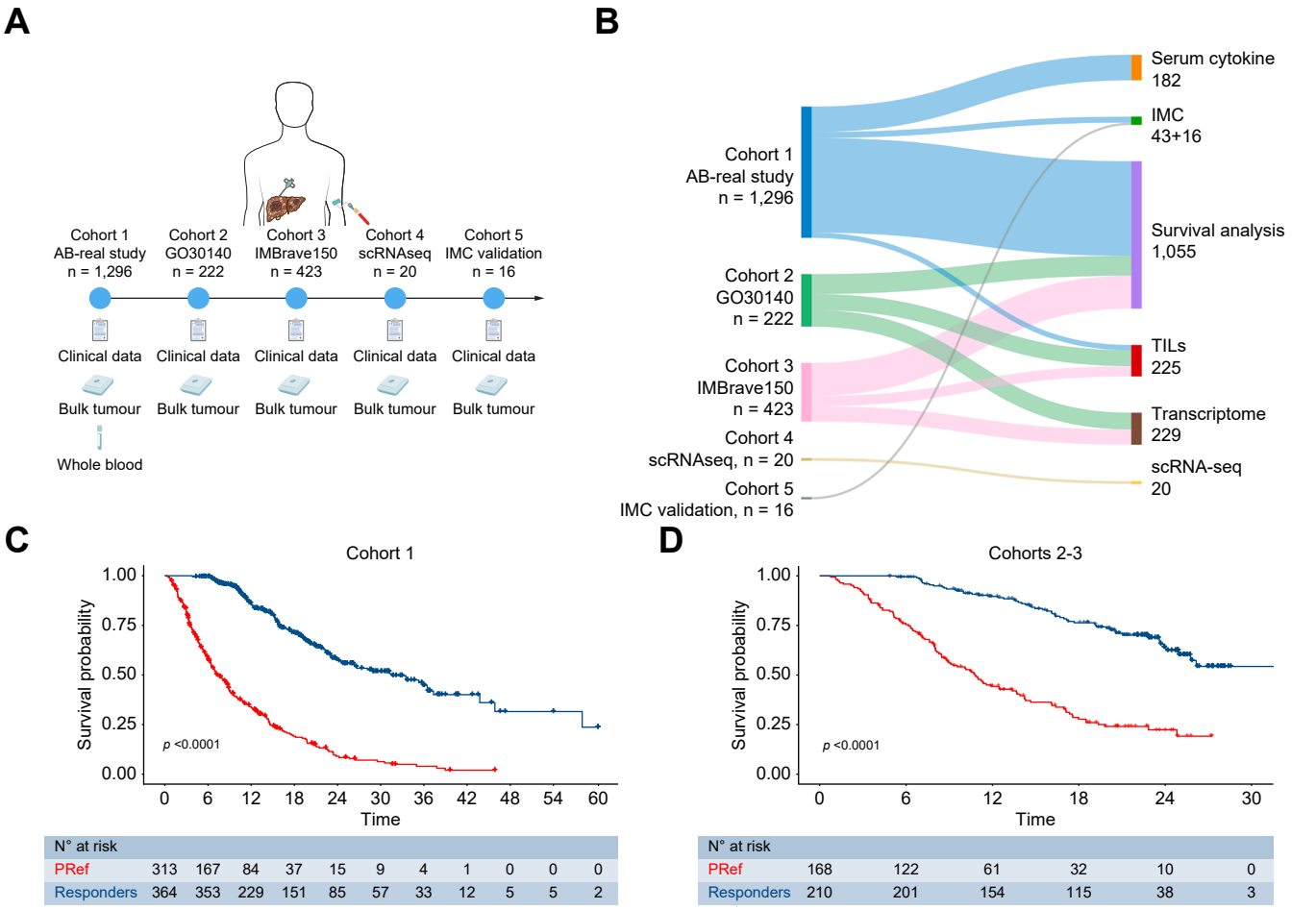

Fig. 1. Study overview. (A) Overview of the five cohorts analysed, comprising 1,296, 222, 423, 20 and 16 patients, respectively. (B) Sample utilisation from each cohort. (C) Kaplan-Meier curves of OS in Cohort 1 stratified by PRef and response (p <0.0001). (D) Kaplan-Meier curves of OS in Cohorts 2-3 stratified by PRef and response (p <0.0001). Threshold for significance: $p \leq 0.05$ (log-rank test). AB, atezolizumab + bevacizumab; IMC, imaging mass cytometry; OS, overall survival; PRef, primary refractoriness; TILs, tumour-infiltrating lymphocytes.

algorithm, with patient identity treated as the batch variable. After quality control, 25,834 cells were retained for analysis, including B cells, myeloid cells, NK cells and T cells. Within the myeloid compartment, unsupervised clustering identified macrophage subsets that were stratified according to CD163 expression levels into CD163$^-$, CD163$^+$int and CD163$^+$high populations for downstream analyses. Detailed analytical procedures are provided in the supplementary methods.

Tissue gene expression analysis

Differential gene expression analysis was performed with DESeq2, comparing responders and PRef. Significant differential expression was defined as an absolute $\log_2$ fold-change of >1 and an adjusted p <0.05.

xCell deconvolution analysis was applied to baseline RNA-seq data, and cell type enrichment scores were compared between PRef and responders using Student's t test with Benjamini–Hochberg correction.

We calculated gene signature scores for each sample as the arithmetic mean of $\log_2$(counts per million) expression of all genes in a given signature (Table S3). Gene set enrichment analysis (GSEA) was performed using the MultiGSEA package (v1.1.99) with default parameters. The analysis employed the Hallmark gene set collection from MSigDB and the CAMERA method for multiple hypothesis testing.

Statistical analysis

Statistical analyses were performed using R v.4.3.1. Survival curves were estimated using the Kaplan-Meier method and compared with the log-rank test. Hazard ratios (HR) with 95% CIs and p values were determined using a stratified Cox proportional hazards model and log-likelihood test. The proportional hazards assumption was validated using Schoenfeld residuals. Multivariate adjustment included key clinical and laboratory variables, detailed in the supplementary methods. To assess the association between SITC-defined response and survival outcomes while minimizing immortal time bias, we employed a time-dependent Cox proportional hazards model. Response status was treated as a time-varying variable, with patients initially classified as PRef. Those who remained progression free after 6 months were reclassified as responders, while others remained PRef. This approach improved the

accuracy of hazard estimates and prevented artificial survival advantages.

To explore determinants of PRef, we applied a conditional inference tree (CTree) analysis (party R package), depicted with Sankey diagrams. The biomarker-evaluable population was analysed separately in Cohorts 2 and 3 to mitigate batch effects in RNA-seq data but was combined for CTree analysis, where RNA signatures were reduced to categorical variables. Further details are provided in the supplementary methods.

Results

Patient cohorts

Of the five patient cohorts derived from prospective observational and randomized clinical studies (Fig. 1A), Cohort 1 consisted of 1,296 patients included in the prospectively maintained database AB-real, a subgroup of whom had pre-treatment tissue available for IMC (n = 43) and serum available for cytokine/chemokine quantification (n = 182). Cohorts 2 and 3 included 645 patients treated in the GO 30140 (n = 222) and IMbrave 150 (n = 423) clinical trials, respectively, with bulk transcriptome data and tumour-infiltrating lymphocyte (TIL) quantification (n = 229 and n = 184, respectively). Cohort 4 comprised 20 patients with advanced HCC and pre-treatment tumour-derived scRNA-seq data available for myeloid cell characterisation. Cohort 5 consisted of 16 patients with pre-treatment tissue available for IMC validation (Fig. 1B). After removing patients who did not meet inclusion criteria, 677 and 378 patients were evaluated for SITC criteria for Cohorts 1 and 2-3, respectively (Fig. S1).

Primary refractoriness to A+B is associated with poor oncological outcomes in unresectable HCC

We first assessed the relationship between PRef and OS, using Cohort 1 as a training set and Cohorts 2-3 as a validation set.

Among the 677 patients in Cohort 1, 313 (46%) were classified as PRef due to progressive disease as first response (220, 70.3%) or stable disease <6 months (93, 29.7%). In Cohorts 2-3, 168 (44%) patients were identified as PRef due to progressive disease (91, 54.2%) or stable disease <6 months (77, 45.8%). Clinical characteristics and outcomes are summarised in Tables S4–6 and the supplementary results.

After a median follow-up of 20.9 (95% CI 19.8–22.0) (Cohort 1) and 14.3 (95% CI 8.1–21.1) months (Cohorts 2-3), 308 (45.9%) patients and 207 (54.8%) patients were alive at the data cut-off in Cohort 1 and Cohorts 2-3, respectively. Median OS was significantly worse in patients with PRef *vs.* responders (Cohort 1: 7.3 *vs.* 31.5 months, HR 3.7, 95% CI 2.8–8.5, p <0.0001; Cohorts 2-3: 10.8 *vs.* not reached, HR 4.6, 95% CI 3.3–6.3, p <0.0001, Fig. 1C,D). To address the risk of immortal time bias, we performed time-dependent multivariate models, which confirmed PRef status to be associated with the highest risk of mortality across Cohorts (Cohort 1: HR 4.0, 95% CI 2.8–5.5, p <0.001; Cohorts 2-3: HR 4.9, 95% CI 3.6–6.7, p <0.001) alongside NLR ≥3, alpha-fetoprotein and albumin-bilirubin (ALBI) grade (Table S7).

To further investigate the clinical characteristics of PRef, the NLR was chosen as a marker of systemic inflammation.[18] Patients with PRef exhibited a higher baseline inflammatory status than responders, as reflected by higher median NLR values (3.6 *vs.* 2.7 in Cohort 1 and 3.3 *vs.* 2.4 in Cohorts 2–3; p <0.001) (Table S4–S6).

PRef is independent of pre-treatment TIL density

We sought to determine whether patients with PRef harboured a differentially immunogenic TME compared to responders and first investigated differences in TIL density across groups, given that TILs are considered *bona fide* markers of spontaneously immunogenic tumours.[19] We applied a pre-optimised machine learning algorithm to evaluate the differential density of TILs in a total of 37 patients treated with A+B in Cohort 1 and 184 patients accrued in Cohorts 2-3 who had digitally available H&E slides. Median cell density was 141 (IQR 419) and 417 (IQR 494) cells/mm^2 of assayed tissue in Cohort 1 and Cohorts 2-3, respectively, and not different in patients with PRef compared to responders (Cohort 1: 138 *vs.* 169 cells/mm^2, p = 0.74, n.s.; Cohorts 2-3 442 *vs.* 399 cells/mm^2, p = 0.57, n.s.; Fig. 2A,B).

PRef to A+B is associated with a unique immune composition of the HCC TME

We next performed in-depth spatial immune phenotyping of the TME to characterise the mechanisms underpinning PRef to A+B. We performed highly multiplexed IMC in a subset of Cohort 1 patients with pre-treatment FFPE tissue available for analysis (n = 43) (Fig. 2C,D). Quantification of major cellular compartments showed no difference in the number of tumour, stromal, endothelial or immune cells in patients with PRef compared to responders (Fig. 2E–H). However, when we compared the abundance of individual cell types, we found that CD163$^+$ tumour-associated macrophages (CD163$^+$ TAMs), encompassing the entire spectrum of CD163 high (CD163^{Hi}) and CD163 intermediate (CD163^{Int}) expression, were enriched in patients with PRef, with the CD163^{Int} TAMs being the individual cell subpopulation most strongly associated with PRef (p <0.0001). These were followed by vascular cancer-associated fibroblasts (vCAFs) (p <0.05). Moreover, although not statistically significant, anti-tumour entities like CD8$^+$ T cells, CD4$^+$ T helpers, dendritic cells (DCs) and CD16^{hi} CD56^{dim} NK cells were enriched in responders, whereas pro-tumour cell types such as neutrophils, CD4$^+$FoxP3$^+$ regulatory T cells (FoxP3$^+$ Treg) and a diversity of other CAF subtypes were enriched in PRef (Figs 3A,B and S2B). In addition, the vCAF/endothelia and Treg/T effector (Teff) cell ratios were significantly higher in those with PRef *vs.* responders (p <0.01 in both cases, Fig. 3C,D). To explore the relationships among key immunosuppressive populations, we performed correlation analyses between CD163^{Int} TAMs, vCAFs and the Treg/Teff cell ratio against all other cell types within the TME. CD163^{Int} TAM density positively correlated with vCAFs, Treg, CD163^{Hi} TAMs and FAP$^+$ myofibroblastic CAFs, while the Treg/Teff cell ratio showed strong positive associations with CD163^{Int} TAMs and vCAFs (Fig. S4A), suggesting a coordinated immunosuppressive network in PRef tumours.

To provide molecular resolution of the TAM subsets identified by IMC, we interrogated single-cell RNA-seq data from Cohort 4 (Fig. S4B and C). Analysis of the myeloid compartment identified macrophage populations that were stratified according to CD163 expression levels into CD163–, CD163^{Int} and CD163^{Hi} TAMs (Fig. 3E). Density analysis showed a higher proportion of CD163^{Int} TAMs in PRef than in responders,

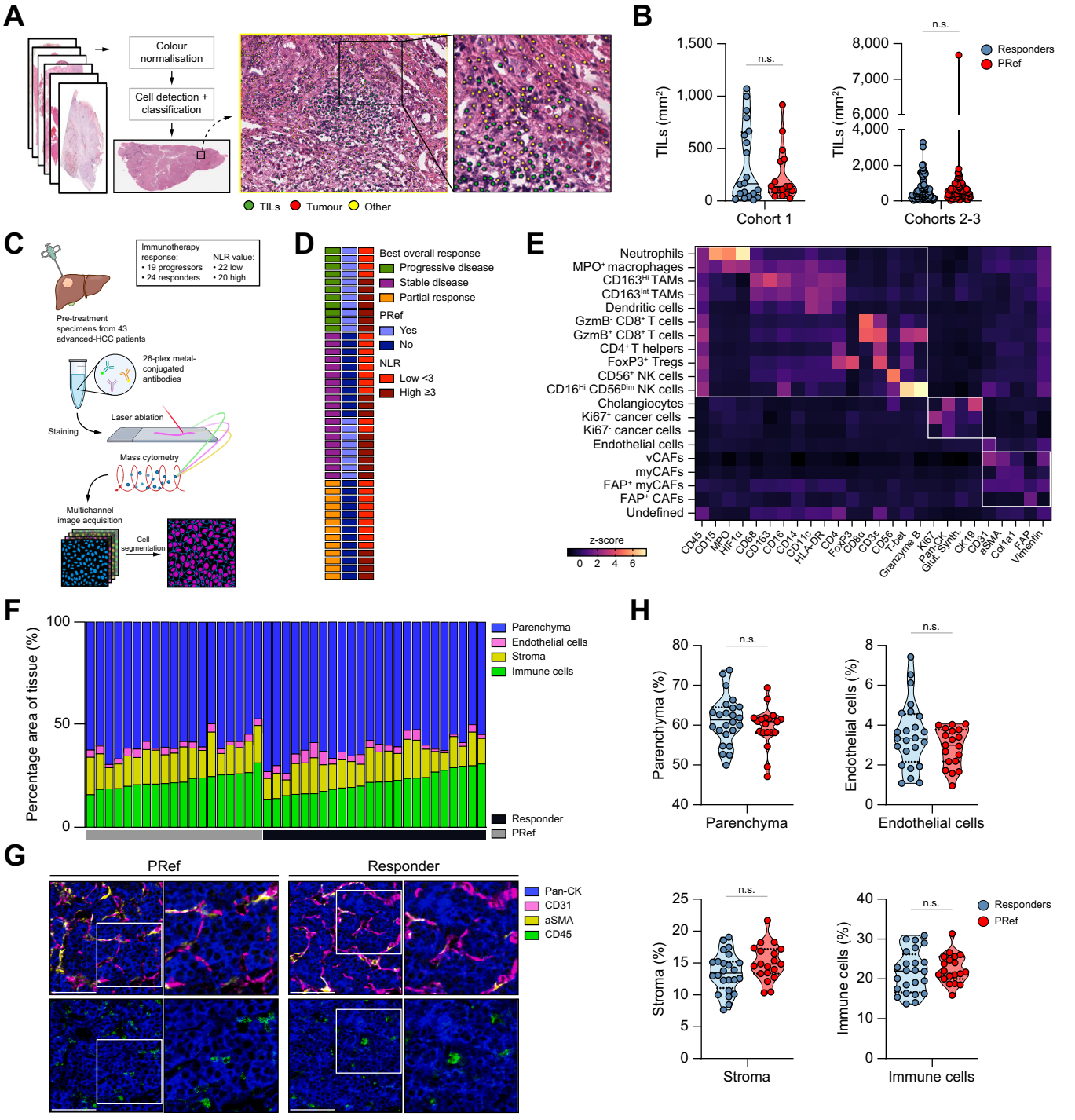

Fig. 2. Decoding the HCC TME of PRef and responders to atezolizumab plus bevacizumab. (A) Schematic of the machine learning-based TIL quantification. (B) TIL counts between patients with PRef and responders in Cohort 1 ($p = 0.74$, n.s.) and Cohorts 2-3 ($p = 0.57$, n.s.). (C-D) IMC cartoon and clinical information of the cohort for response, PRef and NLR. (E) Identity HeatMap showing the cell types identified in the HCC TME by IMC. (F–H) IMC data and representative figures for the comparison of whole parenchyma, endothelia, stroma and immunity between those with PRef and responders. Threshold for significance: $p \leq 0.05$ (non-parametric unpaired Mann-Whitney test). CAFs, cancer-associated fibroblasts; MPO, myeloperoxidase; myCAFs, myofibroblast CAFs; NLR, neutrophil to lymphocyte ratio; NK, natural killer; PanCK, pan-cytokeratin; TAMs, tumour-associated macrophages; TME, tumour microenvironment; vCAFs, vascular CAFs.

consistent with our IMC findings. Evaluation of macrophage polarisation markers revealed that CD163^{Int} TAMs expressed high levels of SPP1 relative to CXCL9, whereas CD163^{Hi} TAMs showed reduced SPP1 expression (Fig. 3E). We also characterised the transcriptional profiles of these macrophage populations by examining the expression of selected functional markers across subsets (Fig. S4D). CD163^{Int} TAMs were characterised by higher expression of TREM2, SPP1 and APOC1, while CD163^{Hi} TAMs showed higher expression of IL-6, CD74 and FOLR2. These findings define distinct

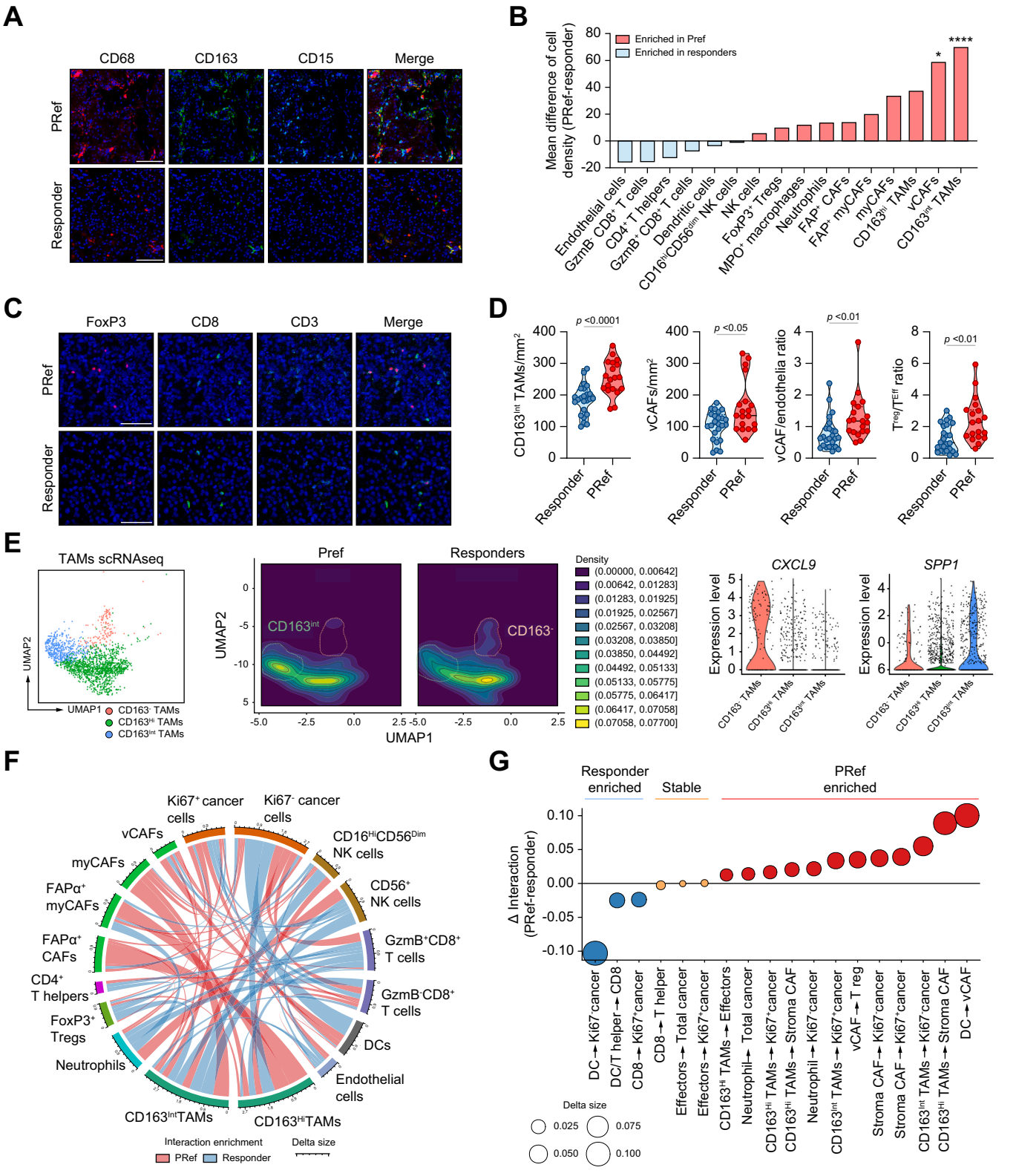

Fig. 3. Immune, stromal and spatial interaction landscape of PRef to atezolizumab plus bevacizumab. (A-B) CD163^{Int} TAMs and vCAFs are enriched in PRef (CD163^{Int} TAMs p <0.0001; vCAFs p <0.05). The scale bar indicates 100 μm. Fig. 3B shows the mean difference of every cell type for patients with PRef *vs.* responders. (C) Treg/Teff cell ratio in those with PRef *vs.* responders (p <0.01). (D) vCAF/endothelia ratio in those with PRef *vs*. responders (p <0.01). (E) Single-cell RNA sequencing analysis of macrophage subsets from Cohort 4: UMAP embedding of CD163–, CD163^{Int} and CD163^{Hi} TAMs (left), density distributions in patients with PRef *vs*. responders (middle), and expression of *CXCL9* and *SPP1* across TAM subsets (right). (F) Chord diagram of cell-cell spatial interactions in PRef and responder tumours; edge colour indicates enrichment in PRef (red) or responders (blue), edge thickness reflects interaction magnitude. (G) Delta difference of spatial interactions (PRef – responder) for interaction modules; positive values indicate enrichment in PRef; bubble size proportional to absolute delta. Threshold for significance: p ≤0.05

transcriptional profiles across CD163^{Int} and CD163^{Hi} macrophage subsets, suggesting a shift in macrophage polarisation across TAM subsets within the TME.

Spatial interaction analysis reveals a PRef-specific immunosuppressive interaction network

To characterise the spatial organisation of these immunosuppressive networks, we performed cell-cell interaction analysis comparing PRef and responder tumours (Fig. 3F,G). PRef tumours were specifically enriched for contacts between immunosuppressive cells (CD163^{Hi} and CD163^{Int} TAMs, neutrophils, stromal CAFs, vCAFs) and both cancer cells and immune regulatory populations, while responder tumours were enriched for effector-to-cancer cell contacts, DC immunosurveillance and CD8 activation (effectors→cancer cells, DC→Ki67– cancer cells, T helper→CD8, DC→CD8). CD163^{Hi} TAMs engaged with the total pool of effector cells, stromal CAFs and cancer cells, whereas CD163^{Int} TAMs interacted with stromal CAFs and cancer cells but not with effectors, indicating a more restricted interaction repertoire consistent with an earlier stage of functional specialisation. Notably, vCAFs constituted a functionally distinct interaction module from stromal CAFs, engaging with Tregs and DCs rather than directly with cancer cells. Additionally, neutrophil-cancer cell spatial interactions were enriched in PRef. The PRef-associated spatial interactions involving CD163^{Hi} and CD163^{Int} TAMs were independently validated in Cohort 5, confirming the reproducibility of the myeloid-driven interaction architecture identified in Cohort 1 (Fig. S4F).

Systemic inflammation mirrors intratumoural immunosuppressive architecture

Because PRef was associated with higher levels of systemic inflammation, we contrasted the TME characteristics of patients with NLR ≥3 and <3. Patients with peripheral blood NLR ≥3 harboured tumours with higher neutrophil/lymphocyte infiltration within the HCC TME (p <0.01) (Fig. 4A–C).

Cell-cell interaction analysis revealed that NLR-high tumours were enriched for interactions of CD163^{Int} TAMs, neutrophils and stromal CAFs with cancer cells, and vCAFs with Tregs and DCs (Figs 4D and S5A,B), partially recapitulating the PRef interaction network. Direct comparison of spatial interaction enrichment between the PRef/responder and NLR-high/NLR-low classifications revealed a significant positive correlation (linear regression p <0.05, Fig. 4E), demonstrating that PRef-enriched interactions were preferentially found in NLR-high patients. This provides a link between systemic inflammation and the immunosuppressive TME architecture characteristic of primary refractoriness.

To further characterise the relationship between PRef and systemic inflammation, we measured a panel of baseline serum cytokines in a subset of Cohort 1 patients (Fig. S6). Among these, IL-6, a pro-inflammatory cytokine and a well-established marker of resistance to immunotherapy in both tissue and blood,[20] was present at higher concentrations in patients with PRef *vs.* responders (p <0.01) (Fig. 4F). Additionally, patients with higher IL-6 levels had reduced OS and progression-free survival compared to those with lower IL-6 levels (Figs 4G and S5C).

Immunosuppressive myeloid cell infiltration is a robust hallmark of PRef to A+B and impairs prognosis

To validate the myeloid/T cell imbalance seen in PRef identified in Cohort 1, we used bulk RNA-seq data from pre-treatment tumour samples from Cohorts 2 and 3. Demographic and baseline characteristics of the biomarker-evaluable patients were generally consistent with those in the whole population recruited to the GO30140 and IMBrave150 trials (Table S8) and so were clinical outcomes (Figs. S7 and S8).

To identify distinctive molecular drivers of PRef, we performed genome-wide differential expression analysis in Cohort 2 (n = 119) as a discovery cohort, and independently validated the findings in Cohort 3 (n = 110). We identified differentially expressed genes specifically dysregulated in patients with PRef compared with responders, enriched for pathways related to immunosuppression and senescence. These included repression of T-cell effector genes including *IFNG*, *GZMB*, *CD8A* and *FASLG* transcriptional traits predictive of immunotherapy response.[21–23] PRef samples were also characterised by a complex gene expression profile with upregulation of immunosuppressive transcripts involved in myeloid infiltration (*i.e.* S100A9, CXCL5, NOS2), systemic inflammation and Treg infiltration (*i.e. IL-6, AREG*), evasion from phagocytosis (*i.e. CD24*), stromal activity (*i.e.* ACTA1), hypoxia and acidosis (*i.e.* CA12, ATP6V1B1), and microenvironment alteration (*i.e. APOA4*). While responders possessed an enrichment in T and NK cell identity plus activation transcripts (*i.e.* CD8A, NCR1, NCAM1, NKG7, GZMB, FASLG, TXK, IFNG), antigen presentation (*i.e.* HLA-DQA1) and anti-tumour myeloid activity (CXCL9). These findings were supported by hallmark GSEA, which confirmed that PRef samples harbour a significant enrichment of immunosuppressive pathways including TNF-α, TGF-β, Notch, and signatures related to epithelial-mesenchymal transition, angiogenesis and hypoxia. In contrast, responders exhibited significant upregulation of gene expression profiles relating to adaptive immunity, such as IFN-α and IFN-γ, suggesting an imbalance in intrinsic tumour immunogenicity between patient groups (Fig. 5A,B).

We then analysed immune signatures in Cohort 2, observing a significant reduction in key immune effector populations, including IFN-γ (p <0.001), Teff (p <0.05), NK (p <0.05) and cytotoxic T (p <0.05) signatures (Figs 5C and S10). While no significant differences were observed in M1/M2 TAM signatures (Fig. S10), we assessed the CXCL9:SPP1 ratio, a recently identified marker of macrophage polarity. We observed differential expression in our Cohort, with PRef characterised by a low CXCL9:SPP1 ratio (p <0.05) (Fig. 5D), consistent with hypoxia-driven immunosuppression and tumour progression. We also observed a significantly higher myeloid:Teff cell ratio (p <0.001) and myeloid-derived

(non-parametric unpaired Mann-Whitney test; permutation-based pairwise interaction analysis for spatial interactions). CAFs, cancer-associated fibroblasts; DC, dendritic cell; NK, natural killer; TAMs, tumour-associated macrophages; Teff, T effector; TME, tumour microenvironment; Treg, T regulatory; UMAP, uniform manifold approximation and projection; vCAFs, vascular CAFs.

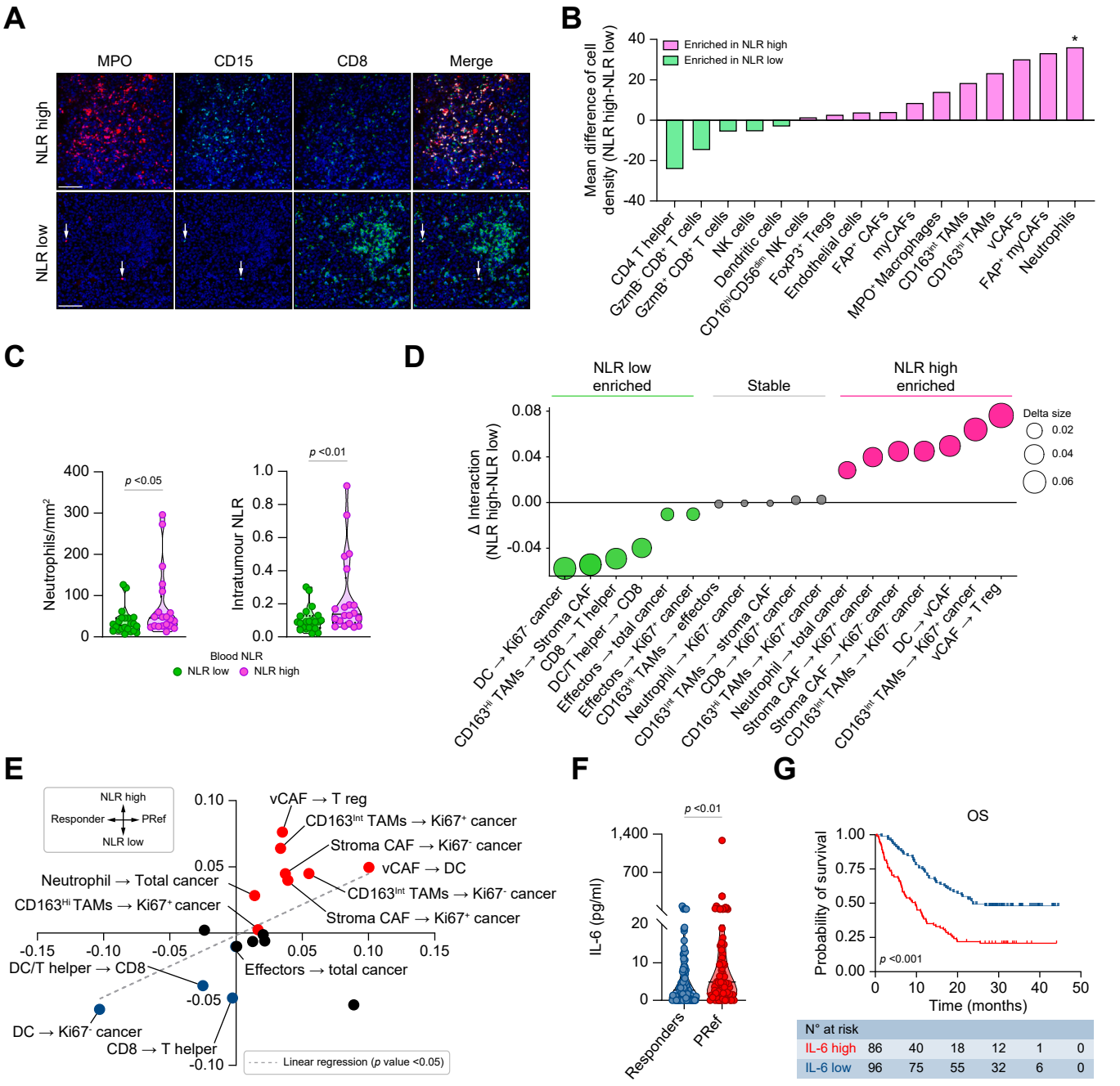

Fig. 4. Systemic inflammation mirrors intratumoural immunosuppressive architecture. (A-B) Patients with high systemic NLR harbour tumours with significantly expanded neutrophils (p <0.01). The scale bar indicates 100 μm. (C) Patients with high systemic NLR also have a high tumour NLR. (D) Delta difference of spatial interactions (NLR-high – NLR-low) for interaction modules. (E) Scatter plot comparing delta interaction enrichment in PRef *vs*. responder (x-axis) and NLR-high *vs*. NLR-low (y-axis; linear regression p <0.05). (F) Serum IL-6 levels in PRef *vs*. responders (p <0.01). (G) Kaplan-Meier curves of OS stratified by high *vs*. low serum IL-6 levels. Threshold for significance: p ≤0.05 (non-parametric unpaired Mann-Whitney test; linear regression for correlation analysis; log-rank test for survival curves). CAFs, cancer-associated fibroblasts; DC, dendritic cell; MPO, myeloperoxidase; NLR, neutrophil to lymphocyte ratio; OS, overall survival; PRef, primary refractoriness; TAMs, tumour-associated macrophages; Treg, T regulatory; vCAFs, vascular CAFs.

suppressor cell (MDSC)/Teff cell ratio (p <0.001) (Fig. 5E–F), confirming the IMC data.

Gene expression signatures associated with PRef are specific to ICI-based therapy

Then, we aimed to validate these signatures in Cohort 3. We observed a significant reduction in key immune effector populations, including IFN-γ (p <0.001), Teff (p <0.05), cytotoxic T (p <0.05) and CXCL9:SPP1 ratio (p <0.05), as well as a significantly higher myeloid:Teff cell ratio (p <0.05) in patients with PRef.

To assess whether the gene expression signatures associated with PRef were specifically predictive of resistance to A+B or represented general prognostic markers, we conducted an exploratory analysis in patients treated with

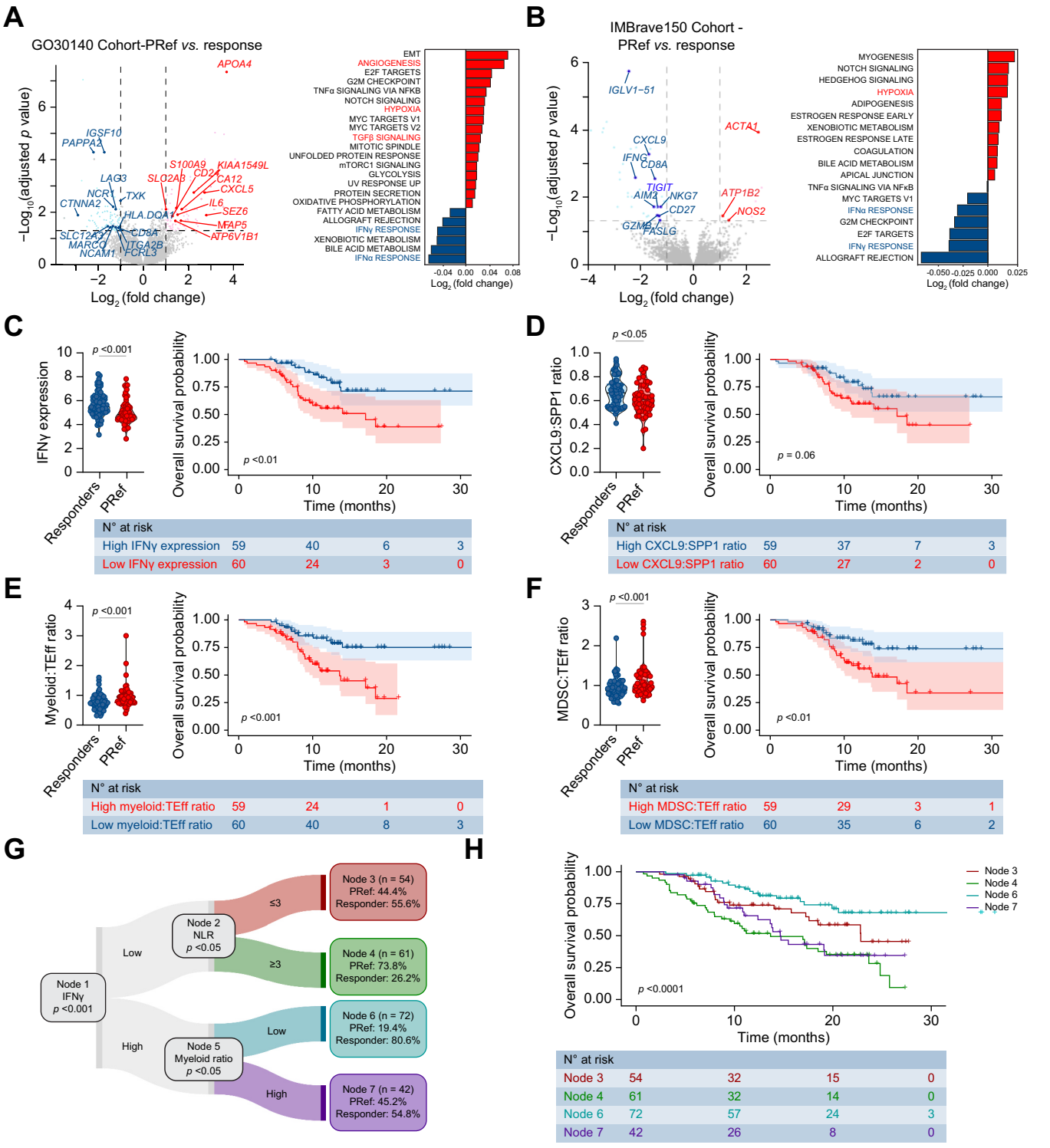

Fig. 5. Gene expression profiles of myeloid immunosuppression in PRef. Differential gene expression (volcano plot) and biological pathways (GSEA by CAMERA of the contrast model in the Hallmark gene set collection) comparing PRef and responders in Cohort 2 (A) and Cohort 3 (B). (C) IFN-γ signature in PRef *vs.* responders (p <0.001) and Kaplan-Meier curve stratified by median expression (p <0.01). (D) CXCL9:SPP1 ratio in PRef *vs.* responders (p <0.05) and Kaplan-Meier curve (p = 0.06). (E) Myeloid:Teff cell ratio in PRef *vs.* responders (p < 0.001) and Kaplan-Meier curve (p <0.001). (F) MDSC:Teff cell ratio in PRef *vs.* responders (p <0.001) and Kaplan-Meier curve (p <0.01). (G) Conditional inference tree integrating IFN-γ signature, NLR and myeloid:Teff cell ratio. (H) Kaplan-Meier curves for Nodes 3, 4, 6 and 7 (p <0.001). Threshold for significance: p ≤0.05. (DESeq2 with Benjamini-Hochberg correction, $|\log_2 FC|$ >1 for differential expression; Student's t test with Benjamini-Hochberg correction for signature comparisons; log-rank test for survival curves; conditional inference tree with Bonferroni-adjusted p values, alpha = 0.05). MDSC, myeloid-derived suppressor cell; NLR, neutrophil to lymphocyte ratio; Teff, T effector.

sorafenib enrolled in Cohort 3 (Table S9). These patients were classified according to SITC criteria.

However, none of these signatures showed any association with PRef in sorafenib-treated patients (all p >0.1) (Table S12).

The TME immune contexture typically associated with PRef is independently associated with poor patient survival

We next evaluated whether the immune signatures defining PRef were independently associated with patient survival. Patients with low expression of the IFN-γ, and Teff signatures, along with high MDSC:Teff and myeloid:Teff cell ratios, had significantly worse OS (IFN-γ signature: HR 2.82, 95% CI 1.42–5.6, p <0.05; Teff signature: HR 2.27, 95% CI 1.16-4.46, p <0.05: MDSC:Teff cell ratio signature: HR 2.54, 95% CI 1.28–5.04, p <0.05; myeloid:Teff cell ratio signature: HR 3.11, 95% CI 1.56–6.2, p <0.001, Figs 5C,E-F, S10C and S11).

Model-based recursive partitioning identifies systemic inflammation and depleted tumour immunogenicity as determinants of PRef to A+B

To verify the relative contribution of routine pre-treatment variables over the underlying tumour immune contexture as a determinant of PRef to A+B, we integrated clinical and transcriptome data from Cohorts 2 and 3 using a CTree.

We selected NLR and ALBI given their independent prognostic role and combined these with IFN-γ, and Teff signatures, along with the MDSC:Teff and myeloid:Teff cell ratio signatures, based on the prognostic relevance demonstrated before. Alpha-fetoprotein levels were excluded due to the high proportion (>50%) of missing values in the biomarker-evaluable patients.

This analysis provided a hierarchical disposition of characteristics independently associated with PRef. Notably, repression of IFN-γ-related transcripts emerged as the most significant factor associated with PRef, especially when combined with high systemic inflammation, as indicated by an NLR ≥3, accounting for 73.8% of the risk of PRef in these patients. Conversely, IFN-γ signature overexpression did not entirely preclude PRef, especially in patients with an elevated myeloid:Teff cell ratio, which doubled the risk compared to those with lower ratios (45% *vs.* 19.4%, Fig. 5G). Consistent with these findings, Kaplan–Meier survival analysis demonstrated significantly different OS outcomes across the identified patient subgroups (Fig. 5H).

Discussion

In a rapidly expanding treatment landscape, where multiple ICI combinations and TKIs are available for unresectable advanced HCC, early identification and mechanistic understanding of primary resistance represent a clinical imperative to broaden the benefit of anti-cancer immunotherapy in HCC.

Leveraging large, globally accrued patient datasets, including landmark clinical trials of A+B, our study provides robust and validated criteria to define primary therapeutic resistance to A+B. We found that PRef, defined as early disease progression or short-lived disease stabilisation, affects approximately 45% of patients treated with A+B in clinical trials and routine practice.

This sizeable subgroup exhibits distinctive clinical and immunological features. PRef was more likely in patients with advanced-stage HCC and was associated with worse ALBI grade and elevated NLR. Hypoalbuminemia and high NLR, two recognised biomarkers of systemic inflammation,[24,25] were strongly associated with PRef, suggesting an unopposed pro-inflammatory milieu. Consistent with these findings, patients with PRef exhibited higher intratumoural expression and elevated circulating IL-6, a cytokine orchestrating the switch from acute to chronic inflammation, reinforcing the link between systemic inflammation and an immune microenvironment polarised towards an immunosuppressive status.[20]

Given the strong association between PRef and systemic inflammation, we next examined the TME to dissect the immune landscape underlying treatment failure. Using IMC on pre-treatment biopsies, we found that PRef tumours were characterised by significantly denser myeloid infiltration, T-cell depletion and a more immunosuppressive TME. The presence of a myeloid-dominant phenotype was independently validated in clinical trial cohorts, demonstrating that PRef represents a distinct IFN-γ-low, myeloid-enriched immune state.

Among myeloid subsets, TAMs emerged as a key determinant of PRef. Our IMC analysis revealed that PRef tumours exhibited an increased density of $CD163^{+}$ TAMs, including both $CD163^{Hi}$ and $CD163^{Int}$ M2-like TAMs, the latter showing the strongest association with PRef. $CD163^{Int}$ TAMs are macrophages that possess both newly recruited and immunomodulatory phenotypes and have previously been implicated in chronic liver disease,[26] likely through effector T-cell suppression. Spatial interaction analysis provided further resolution of TAM function within the PRef microenvironment. We identified a PRef-specific interaction network characterised by hierarchical TAM interactions: $CD163^{Hi}$ TAMs engaged with effector cells, stromal CAFs and cancer cells, while $CD163^{Int}$ TAMs interacted with stromal CAFs and cancer cells but not with effectors, suggesting a maturation-dependent functional specialisation within the TAM compartment. The interaction of both TAM subsets with stromal CAFs is consistent with the recently described $SPP1^{+}$ TAM-CAF axis driving hypoxia-mediated immunosuppression, and aligns with the enrichment of SPP1, TGF-β and hypoxia pathways in PRef transcriptomic profiles.[27] These spatial interactions were reproducible across an independently accrued validation cohort.

Consistent with these spatial findings, the evaluation of macrophage polarisation markers at the transcriptomic level confirmed that PRef tumours exhibited a lower CXCL9:SPP1 ratio, reflecting a shift from anti-tumour IFN-γ-driven CXCL9 polarisation towards pro-tumour hypoxia-driven SPP1 polarisation.[28] Single-cell transcriptomic profiling further refined this observation by demonstrating that $CD163^{Int}$ TAMs, the subset most strongly enriched in PRef tumours, exhibit a transcriptional programme characterised by high SPP1 and TREM2 expression with low CXCL9 levels, while $CD163^{Hi}$ TAMs display increased expression of IL-6 and FOLR2. These findings provide cellular resolution to the bulk transcriptomic CXCL9:SPP1 imbalance. This convergence across spatial proteomics, bulk and single-cell transcriptomics reinforces the myeloid-dominant architecture of primary resistance.

Beyond individual markers, our findings revealed a broader imbalance in the myeloid compartment of PRef tumours. While NLR has long been recognised as a poor prognostic indicator,[29] our study is the first to describe a link between

peripheral NLR and immunosuppressive myeloid cell infiltration within the TME. Beyond this correlation, we demonstrated that the spatial cell-cell interaction programmes enriched in PRef tumours are significantly correlated with those enriched in NLR-high tumours (p <0.05), providing direct evidence that systemic inflammation mirrors specific immunosuppressive interaction architectures within the TME. This finding suggests that NLR may serve not merely as a prognostic indicator but as a peripheral surrogate of the intratumoural immunosuppressive network, and may pave the way for neutrophil-targeted therapies currently in clinical trials to overcome ICI resistance.[30–32]

Whilst independently associated with prognosis and refractoriness to treatment, the systemic pro-inflammatory response associated with PRef is known to be conditioned by redundant and pleiotropic molecular drivers. For this reason, we opted to integrate findings from our transcriptomic experiments and clinical data to define the hierarchical relationships among resistance mechanisms. Using CTree, we identified IFN-γ repression as the primary determinant of PRef risk, particularly in the presence of elevated systemic inflammation (NLR ≥3). The presence of these two independent traits defined a high-risk subgroup with a 74% probability of PRef, representing the most unfavourable biological scenario. Notably, even among patients with high IFN-γ expression, an elevated myeloid:Teff cell ratio more than doubled the risk of PRef (45% *vs.* 19.4%), underscoring the critical role of the balance between effector and suppressive immune populations in shaping treatment outcomes. This hierarchical model not only provides deeper insights into resistance mechanisms but also supports patient stratification based on the dominant resistance pathway, with potential implications for personalised therapeutic strategies.

Several limitations of our study should be acknowledged. Although our multi-cohort approach provides robust validation of the determinants and clinical characteristics of patients with PRef to A+B, the retrospective nature of the study makes it susceptible to selection bias, particularly within the observational cohort. While convergent, IMC and transcriptomic analyses were conducted on different patient subsets with non-overlapping experimental readouts and limited sample sizes, potentially limiting direct cross-comparisons and warranting interpretation of these findings as hypothesis-generating. Additionally, detailed histopathological data, including Edmondson grade and histological subtype, were not systematically available for the biomarker-evaluable population, precluding assessment of whether differences in immune cell composition may partly reflect tumour differentiation status. While we identified key biological features associated with PRef, the causal relationships among these factors remain to be fully elucidated. Furthermore, as our findings are derived exclusively from patients treated with A+B, whether the biological determinants of PRef identified here generalise to other ICI-based regimens, such as durvalumab plus tremelimumab or nivolumab plus ipilimumab, remains to be established, and validation in these settings would further strengthen the broader applicability of our conclusions. Beyond the core immune signals, broader pathway-level findings from GSEA were not uniformly replicated in the validation cohort and should be considered exploratory. Lastly, while our conditional inference tree model offers a framework for patient stratification, prospective validation in independent cohorts is necessary before clinical implementation.

Despite these limitations, our findings have significant implications for drug development and study design in HCC. The prominence of myeloid-mediated immunosuppression suggests that targeting this axis could enhance the efficacy of A+B. Several emerging therapeutic strategies aim to counteract myeloid-driven resistance by modulating macrophage and myeloid cell function within the TME, including the combination of A+B with anti-TIGIT inhibitors.[33] Other strategies to overcome myeloid-driven tumour immune escape may involve blocking LILRB2 (ILT4), known to transmit inhibitory signals in macrophages[34] (NCT04524871); the use of CXCR2 inhibitors, which deplete or reprogramme immunosuppressive neutrophils (EudraCT 2020-003346-3631433989); or SPP1 neutralising agents, which are currently in pre-clinical experimental stages.[35] Our hierarchical model suggests that patients with repressed IFN-γ signalling and NLR ≥3, who have a 74% probability of PRef, may represent prime candidates for myeloid-targeting combination strategies; notably, while NLR is readily available from routine blood counts, clinical implementation of IFN-γ assessment will require validation of FFPE-compatible platforms or immunohistochemistry-based surrogate markers.

In conclusion, our study provides the first comprehensive characterisation of PRef to A+B in HCC, establishing PRef as a distinct biological entity defined by systemic inflammation, myeloid cell infiltration, and T-cell depletion. These findings not only enhance our understanding of immunotherapy resistance in HCC but also lay the groundwork for biomarker-driven combination strategies aimed at overcoming primary resistance, a strategy to be evaluated prospectively in future studies.

Affiliations

[1]*Department of Surgery & Cancer, Imperial College London, Hammersmith Hospital, Du Cane Road, London, UK;* [2]*Phase 1 Unit, Fondazione Policlinico Universitario A. Gemelli, IRCCS, Università Cattolica del Sacro Cuore, Rome, Italy;* [3]*The Newcastle University Centre for Cancer, Newcastle University, Newcastle Upon Tyne, UK;* [4]*Department of Translational Medicine, Università del Piemonte Orientale, Novara, Italy;* [5]*Image Analysis Unit, Faculty of Medical Sciences, Newcastle University, Newcastle Upon Tyne, UK;* [6]*Digestive Oncology, Department of Gastroenterology and Hepatology, UZ/KU Leuven, Belgium;* [7]*Section of Gastroenterology & Hepatology, Department of Health Promotion, Mother and Child Care, Internal Medicine and Medical Specialties, PROMISE, University of Palermo, Palermo, Italy;* [8]*Department of Medical and Surgical Sciences, University of Bologna, Italy;* [9]*Medical Oncology, Department of Internal Medicine, CHA Bundang Medical Center, CHA University, Seongnam, Republic of Korea;* [10]*Department of Medicine, Division of Hematology/Oncology, Tisch Cancer Institute, Mount Sinai Hospital, New York, NY, USA;* [11]*Department of Medicine, Division of Hematology & Oncology, University of Pittsburgh Medical Center, Pittsburgh, PA, USA;* [12]*Division of Gastroenterology and Hepatology, Department of Medicine III, Medical University of Vienna, Vienna, Austria;* [13]*Department of Medical Research, Taipei Veterans General Hospital, Taipei, Taiwan;* [14]*Division of Gastroenterology and Hepatology, Department of Medicine, Taipei Veterans General Hospital, Taipei, Taiwan;* [15]*Institute of Clinical Medicine, National Yang Ming Chiao Tung University, Taipei, Taiwan;* [16]*Department of Gastroenterology and Hepatology, Kindai University Faculty of Medicine, Osaka, Japan;* [17]*Department of Gastroenterology and Hepatology, Chang Gung Medical Foundation, Linkou Chang Gung Memorial Hospital, Taiwan NO 5, Fu-Hsing Street, Kuei Shan, Taoyuan 333, Taiwan;* [18]*University of Verona, Department of Medicine General Medicine C Unit & Liver Unit, Italy;* [19]*Department of Translational Research and New Technologies in Medicine and Surgery, University of Pisa, Pisa, Italy, Unit of Medical Oncology 2, Azienda Ospedaliero-Universitaria Pisana, Pisa, Italy;* [20]*Department of Medicine II (Gastroenterology, Hepatology, Endocrinology and Infectious Diseases), Freiburg*

University Medical Center, University of Freiburg, Freiburg, Germany; [21]*Department of Oncology, Hematology and Bone Marrow Transplantation with Section of Pneumology, University Medical Center Hamburg-Eppendorf, Hamburg, Germany;* [22]*Gastrointestinal Medical Oncology Department, University of Texas MD Anderson Cancer Center, Houston, TX, USA;* [23]*University Medical Center Mainz, I. Dept. of Internal Medicine, Mainz, Germany;* [24]*Department of Internal Medicine, Center for Digestive Medicine, China Medical University Hospital, Taichung, Taiwan;* [25]*Department of Biomedical Sciences, Humanitas University, Via Rita Levi Montalcini 4, 20072 Pieve Emanuele, Milan, Italy;* [26]*Hepatopancreatobiliary Oncology, Humanitas Cancer Center, IRCCS Humanitas Research Hospital, Via A. Manzoni 56, 20089 Rozzano, Milan, Italy;* [27]*Department of Oncology, Università Politecnica delle Marche, Azienda Ospedaliero-Universitaria delle Marche, Ancona, Italy;* [28]*Department of Medicine (Hematology/Oncology), UCSF Helen Diller Family Comprehensive Cancer Center, San Francisco, California, USA;* [29]*Department of Gastroenterology and Hepatology, Ogaki Municipal Hospital, Ogaki, Japan;* [30]*Department of Clinical Pathology, University Hospital of North Norway, Tromsø, Norway;* [31]*Department of Cancer Genetics, Oslo University Hospital, Oslo, Norway;* [32]*Department of Medicine, Brigham and Women's Hospital, Harvard Medical School, Boston, Massachusetts, USA;* [33]*Department of Medical Biology, UiT The Arctic University of Norway, Tromsø, Norway;* [34]*Department of Surgical, Oncological and Oral Sciences (Di.Chir.On.S.), University of Palermo, Italy;* [35]*Division of Internal Medicine, Hepatobiliary and Immunoallergic Diseases, IRCCS Azienda Ospedaliero-Universitaria di Bologna, Italy;* [36]*Department of Pathology, CHA Bundang Medical Center, CHA University School of Medicine, Seongnam, Republic of Korea;* [37]*Department of Biomedical Science, College of Life Science, CHA University School of Medicine, Seongnam, Republic of Korea;* [38]*Division of Gastroenterology and Hepatology, University of California, San Francisco, California, USA;* [39]*Department of Life Sciences, Imperial College London, South Kensington Campus, Exhibition Road, London, SW7 2AZ, UK;* [40]*Research Department of Oncology, UCL Cancer Institute, University College London, Royal Free Hospital, London, UK;* [41]*Newcastle University Translational and Clinical Research Institute, Newcastle Upon Tyne, UK;* [42]*NIHR, Newcastle Biomedical Research Centre, Newcastle University, Newcastle Upon Tyne, Tyne and Wear, UK*

Abbreviations

A+B, atezolizumab plus bevacizumab; ALBI, albumin-bilirubin; CAFs, cancer-associated fibroblasts; CTree, conditional inference tree; DC, dendritic cell; FFPE, formalin-fixed paraffin-embedded; GSEA, gene set-enrichment analysis; HCC, hepatocellular carcinoma; HR, hazard ratio; ICI, immune checkpoint inhibitors; IMC, imaging mass cytometry; MDSCs, myeloid-derived suppressor cells; NLR, neutrophil-to-lymphocyte ratio; OS, overall survival; PRef, primary refractoriness; RNA-seq, RNA sequencing; scRNA-seq, single-cell RNA sequencing; SITC, Society for Immunotherapy of Cancer; TAMs, tumour-associated macrophages; Teff, T effector; TILs, tumour-infiltrating lymphocytes; TKIs, tyrosine kinase inhibitors; TME, tumour microenvironment; Treg, regulatory T; vCAFs, vascular CAFs.

Financial support

This research was funded by the National Research Foundation of Korea (NRF) grants, supported by the Korean government (MSIT): grant numbers NRF 2023R1A2C2004339 to H.J.C. J.L. is supported by an Academy of Medical Sciences Springboard award (SBF009\1103), Royal Society Research Grant (RG\R2\232323), JGW Patterson Foundation primer grant, CRUK program grants (DRCRPG-Nov22/100007) and an MRC project grant (MR/Y003365/1). E.R.G funded by W.E. Harker PhD studentship (C0260N3038). J.L., H.L.R. and E.R.G are supported by a NIHR BRC project grant (NIHR203309). H.L.R. is supported by a CRUK Accelerator award (A26813) and European Commission (Horizon Europe-Mission Cancer, THRIVE, Ref. 101136622). This research was supported by the 'Stichting Tegen Kanker' (FAF-C/2018/1297) grant to J.D.

Conflicts of interest

PL reports an ESMO translational fellowship. ERG reports a W.E. Harker PhD Studentship and a Doctoral College Research Enhancement Fund from Newcastle University. LB reports a Fondazione Bonadonna Fellowship. SC reports consulting fees from AstraZeneca and advisory board fees from AstraZeneca, Merck, and Ipsen. AD reports consulting or advisory board role with MSD/Eisai, AstraZeneca, Roche, and MSD. AT reports a CRUK MBBS/PhD studentship. TUM currently or has previously served on advisory and/or data safety monitoring boards for Rockefeller University, Regeneron, AbbVie, Merck, EMD Serono, Geneos, AstraZeneca, Genentech, Glenmark, Arrowhead, G1 Therapeutics, NGMbio, DBV Technologies, Arcus, Fate, Ono, Storm, Replimmune, Avammune, Tubulis, NaturesToolbox, EvolveImmune, Abdera, AN2 Therapeutics, and Astellas; research grants from NIH (NCI), Cancer Research Institute, Regeneron, Genentech, Bristol-Myers Squibb, Merck, and Boehringer Ingelheim; and holds stock options in Natures Toolbox. AS reports consulting or advisory board role with AstraZeneca, Bristol-Myers Squibb, Merck, Exelixis, Pfizer, Xilio Therapeutics, Taiho, Amgen, Autem Therapeutics, KAHR Medical, Arcus Therapeutics, Regeneron, and Replimune; institutional research funding from AstraZeneca, Bristol-Myers Squibb, Merck, Exelixis, Actuate Therapeutics, Incyte Corporation, Amgen, Oxford Biotherapeutics, Replimune, Phanes Therapeutics, Arcus Therapeutics, Regeneron, and KAHR Medical. MP received speaker honoraria from Bayer, BMS, Eisai, Ipsen, Lilly, MSD, and Roche; is a consultant/advisory board member for AstraZeneca, Bayer, BMS, Eisai, Ipsen, Lilly, MSD, and Roche; received grants from AstraZeneca, Bayer, BMS, Eisai, and Roche; and travel support from Bayer, BMS, Ipsen, and Roche. BS reports institutional grants from AstraZeneca, Eisai, Ipsen, and Roche Diagnostics, and consulting/advisory fees from AstraZeneca, Eisai, Ipsen, Roche, and Gilead. WFH reports speaker honoraria from AstraZeneca, BMS, Gilead, and Roche. PRG reports consulting fees, honoraria, and advisory board fees from Bayer, AstraZeneca, BMS, MSD, and Roche. MK reports institutional research funding and consulting fees/honoraria from Roche, Eisai, and AstraZeneca. LR reports consulting fees from AbbVie, AstraZeneca, Basilea, Bayer, BMS, Eisai, Elevar Therapeutics, Exelixis, Genenta, Hengrui, Incyte, Ipsen, Jazz Pharmaceuticals, MSD, Nerviano Medical Sciences, Roche, Servier, Taiho Oncology, and Zymeworks; lecture fees from AstraZeneca, Bayer, BMS, Guerbet, Incyte, Ipsen, Roche, and Servier; travel expenses from AstraZeneca and Servier; research grants (to institution) from AbbVie, AstraZeneca, BeiGene, Exelixis, Fibrogen, Incyte, Ipsen, Jazz Pharmaceuticals, MSD, Nerviano Medical Sciences, Roche, Servier, Taiho Oncology, TransThera Sciences, and Zymeworks. AP reports grants from Incyte, consulting fees from Taiho, AstraZeneca, Amgen, and MSD, and advisory board fees from Incyte, Taiho, BMS, Merck, Daiichi-Sankyo, and Accord. RKK reports consulting fees from AstraZeneca and Boehringer Ingelheim, institutional grants for clinical trials from Agios, AstraZeneca, Bayer, Genentech/Roche, Merck, Servier, and Taiho, and travel support from Merck and Genentech/Roche. HT reports honoraria from AbbVie, Gilead, Terumo, Fujifilm WAKO, Eisai, AstraZeneca, Kowa, Bayer, and BMS. GC reports advisory board participation and speaker fees from Eisai, AstraZeneca, MSD, Roche, and Gilead. FP reports consulting or advisory board role with AstraZeneca, Bracco, BMS, ESAOTE, Eisai, GE, Gilead, Ipsen, MSD, Nerviano, Roche, Samsung, Signant Health, and Siemens Healthineers. ML reports advisory board fees from AstraZeneca. JD reports grants from AstraZeneca, Roche, and Bayer, and consulting/advisory fees from AbbVie, AstraZeneca, Bayer, BMS, Eisai, Ipsen, Lilly, MSD, Roche, and Servier. TM reports grants from MSD and Bayer, and consulting fees from Roche and Ipsen. HLR reports grants from Cancer Research Horizons. HJC reports grants from Roche and advisory board/honoraria from Eisai, Roche, MSD, BMS, Servier, and AstraZeneca. JL reports grants from the Royal Society, JGW Patterson Foundation, CRUK, and MRC. DJP received lecture fees from Bayer Healthcare, Eisai, BMS, Roche, and Boston Scientific; travel expenses from BMS and Bayer Healthcare; consulting fees from Mina Therapeutics, DaVolterra, Mursla, Ipsen, Exact Sciences, Avamune, Eisai, Roche, Starpharma, LiFT Biosciences, and AstraZeneca; and institutional research funding from MSD, GSK, and BMS. All remaining authors report no conflicts of interest.

Please refer to the accompanying ICMJE disclosure forms for further details.

Authors' contributions

Pasquale Lombardi: Conceptualization, Methodology, Formal Analysis (clinical data, bulk RNA-seq, TILs quantification), Investigation, Data Curation, Writing – Original Draft, Writing – Review & Editing, Visualization, Project Administration. Erik Ramon-Gil: Conceptualization, Methodology, Formal Analysis (imaging mass cytometry, spatial cell-cell interaction analysis), Investigation, Data Curation, Writing – Original Draft, Writing – Review & Editing, Visualization, Project Administration. Rabial Q. Raja: Formal Analysis (spatial cell-cell interaction analysis), Investigation. Leonardo Brunetti: Investigation, Data Curation, Formal Analysis. Giulia Francesca Manfredi: Investigation, Formal Analysis. Zhongguo Zhou: Formal Analysis (single-cell RNA-seq analysis). George Merces: Methodology, Formal Analysis (image segmentation and IMC acquisition). Mehrdad Rakaee and Falah Jabar: Methodology, Formal Analysis (machine learning-based TILs quantification). Hong Jae Chon: Supervision, Writing – Review & Editing, Funding Acquisition. Jack Leslie: Conceptualization, Methodology, Supervision, Formal Analysis, Writing – Review & Editing, Funding Acquisition. David J. Pinato: Conceptualization, Methodology, Supervision, Writing – Original Draft, Writing – Review & Editing, Project Administration, Funding Acquisition. All remaining authors contributed to Investigation, Resources, Data Curation, and/or Supervision through patient recruitment, clinical data collection, provision of

study materials, and/or local oversight. All authors critically reviewed the manuscript and approved the final version.

Data availability

All clinical, raw RNA-seq data for the GO30140 and IMbrave150 trials are deposited in the European Genome-Phenome Archive under accession no. EGAS00001005503. Qualified researchers may request access to individual patient-level data through the clinical study data request platform (https://vivli.org/). Further details on Roche's criteria for eligible studies are available at https://vivli.org/members/ourmembers. For further details on Roche's Global Policy on the Sharing of Clinical Information and how to request access to related clinical study documents, see https://www.roche.com/research_and_development/who_we_are_how_we_work/clinical_trials/our_commitment_to_data_sharing.htm.

Acknowledgements

The authors would like to acknowledge the following sources of funding: European Society of Medical Oncology (ESMO) Translational Fellowship (to PL).

Supplementary data

Supplementary data to this article can be found online at https://doi.org/10.1016/j.jhep.2026.05.018.

References

Author names in bold designate shared co-first authorship

[1] Cheng AL, Qin S, Ikeda M, et al. Updated efficacy and safety data from IMbrave150: Atezolizumab plus bevacizumab *vs.* sorafenib for unresectable hepatocellular carcinoma. J Hepatol 2022;76(4):862–873.
[2] Rimassa L, Chan SL, Sangro B, et al. Five-year overall survival update from the HIMALAYA study of tremelimumab plus durvalumab in unresectable HCC. J Hepatol 2025 Oct;83(4):899–908. https://doi.org/10.1016/j.jhep.2025.03.033. Epub 2025 Apr 11. PMID: 40222621.
[3] Vogel A, Chan SL, Dawson LA, et al. Hepatocellular carcinoma: ESMO Clinical Practice Guideline for diagnosis, treatment and follow-up. Ann Oncol 2025;36(5):491–506.
[4] Fulgenzi CAM, Scheiner B, Korolewicz J, et al. Efficacy and safety of frontline systemic therapy for advanced HCC: a network meta-analysis of landmark phase III trials. JHEP Rep 2023;5(5):100702.
[5] Llovet JM, Castet F, Heikenwalder M, et al. Immunotherapies for hepatocellular carcinoma. Nat Rev Clin Oncol 2022;19(3):151–172.
[6] Sangro B, Chan SL, Kelley RK, et al. Four-year overall survival update from the phase III HIMALAYA study of tremelimumab plus durvalumab in unresectable hepatocellular carcinoma. Ann Oncol 2024;35(5):448–457.
[7] Fulgenzi CAM, Cheon J, D'Alessio A, et al. Reproducible safety and efficacy of atezolizumab plus bevacizumab for HCC in clinical practice: results of the AB-real study. Eur J Cancer 2022;175:204–213.
[8] Campani C, Vallot A, Ghannouchi H, et al. Impact of radiological response and pattern of progression in patients with HCC treated by atezolizumab-bevacizumab. Hepatology 2024;79(1):49–60.
[9] Sharma P, Hu-Lieskovan S, Wargo JA, et al. Primary, adaptive, and acquired resistance to cancer immunotherapy. Cell 2017;168(4):707–723.
[10] Kluger H, Barrett JC, Gainor JF, et al. Society for Immunotherapy of Cancer (SITC) consensus definitions for resistance to combinations of immune checkpoint inhibitors. J Immunother Cancer 2023;11(3).
[11] Celsa C, Cabibbo G, Fulgenzi CAM, et al. Hepatic decompensation is the major driver of mortality in patients with HCC treated with atezolizumab plus bevacizumab: the impact of successful antiviral treatment. Hepatology 2025;81(3):837–852.
[12] Cappuyns S, Pique-Gili M, Esteban-Fabro R, et al. Single-cell RNA sequencing-derived signatures define response patterns to atezolizumab + bevacizumab in advanced hepatocellular carcinoma. J Hepatol 2024 Jun;82(6):1036–1049. https://doi.org/10.1016/j.jhep.2024.12.016. Epub 2024 Dec 19. PMID: 39709141; PMCID: PMC12086051.
[13] Zhu AX, Abbas AR, de Galarreta MR, et al. Molecular correlates of clinical response and resistance to atezolizumab in combination with bevacizumab in advanced hepatocellular carcinoma. Nat Med 2022;28(8):1599–1611.
[14] Lee MS, Ryoo BY, Hsu CH, et al. Atezolizumab with or without bevacizumab in unresectable hepatocellular carcinoma (GO30140): an open-label, multicentre, phase 1b study. Lancet Oncol 2020;21(6):808–820.
[15] Finn RS, Qin S, Ikeda M, et al. Atezolizumab plus Bevacizumab in unresectable hepatocellular carcinoma. N Engl J Med 2020;382(20):1894–1905.
[16] Cappuyns S, Philips G, Vandecaveye V, et al. PD-1(-) CD45RA(+) effector-memory CD8 T cells and CXCL10(+) macrophages are associated with response to atezolizumab plus bevacizumab in advanced hepatocellular carcinoma. Nat Commun 2023;14(1):7825.
[17] Rakaee M, Adib E, Ricciuti B, et al. Association of machine learning-based assessment of tumor-infiltrating lymphocytes on standard histologic images with outcomes of immunotherapy in patients with NSCLC. JAMA Oncol 2023;9(1):51–60.
[18] Manfredi GF, Fulgenzi CAM, D'Alessio A, et al. Identification of factors associated with primary refractoriness to atezolizumab plus bevacizumab in patients with advanced hepatocellular carcinoma. Dig Liver Dis 2024;56:S8–S9.
[19] Presti D, Dall'Olio FG, Besse B, et al. Tumor infiltrating lymphocytes (TILs) as a predictive biomarker of response to checkpoint blockers in solid tumors: a systematic review. Crit Rev Oncol Hematol 2022;177:103773.
[20] Fisher DT, Appenheimer MM, Evans SS. The two faces of IL-6 in the tumor microenvironment. Semin Immunol 2014;26(1):38–47.
[21] Jorgovanovic D, Song M, Wang L, et al. Roles of IFN-gamma in tumor progression and regression: a review. Biomark Res 2020;8:49.
[22] Fumet JD, Richard C, Ledys F, et al. Prognostic and predictive role of CD8 and PD-L1 determination in lung tumor tissue of patients under anti-PD-1 therapy. Br J Cancer 2018;119(8):950–960.
[23] Xiao W, Ibrahim ML, Redd PS, et al. Loss of Fas expression and function is coupled with colon cancer resistance to immune checkpoint inhibitor immunotherapy. Mol Cancer Res 2019;17(2):420–430.
[24] Halazun KJ, Hardy MA, Rana AA, et al. Negative impact of neutrophil-lymphocyte ratio on outcome after liver transplantation for hepatocellular carcinoma. Ann Surg 2009;250(1):141–151.
[25] Forrest LM, McMillan DC, McArdle CS, et al. Evaluation of cumulative prognostic scores based on the systemic inflammatory response in patients with inoperable non-small-cell lung cancer. Br J Cancer 2003;89(6):1028–1030.
[26] Guillot A, Winkler M, Silva Afonso M, et al. Mapping the hepatic immune landscape identifies monocytic macrophages as key drivers of steatohepatitis and cholangiopathy progression. Hepatology 2023;78(1). Baltimore, Md.
[27] Qi J, Sun H, Zhang Y, et al. Single-cell and spatial analysis reveal interaction of FAP(+) fibroblasts and SPP1(+) macrophages in colorectal cancer. Nat Commun 2022;13(1):1742.
[28] **Bill R**, **Wirapati P**, Messemaker M, et al. CXCL9:SPP1 macrophage polarity identifies a network of cellular programs that control human cancers. Science 2023;381(6657):515–524.
[29] Guthrie GJ, Charles KA, Roxburgh CS, et al. The systemic inflammation-based neutrophil-lymphocyte ratio: experience in patients with cancer. Crit Rev Oncol Hematol 2013;88(1):218–230.
[30] Evans TRJ, Basu B, Hubner R, et al. A phase I/II study of the CXCR2 inhibitor, AZD5069, in combination with durvalumab, in patients (pts) with advanced hepatocellular carcinoma (HCC). J Clin Oncol 2023;41(4_suppl). TPS631-TPS631.
[31] Leslie J, Mackey JBG, Jamieson T, et al. CXCR2 inhibition enables NASH-HCC immunotherapy. Gut 2022;71(10):2093–2106.
[32] Ramon-Gil E, Geh D, Leslie J. Harnessing neutrophil plasticity for HCC immunotherapy. Essays Biochem 2023;67(6):941–955.
[33] Han JH, Cai M, Grein J, et al. Effective anti-tumor response by TIGIT blockade associated with FcgammaR engagement and myeloid cell activation. Front Immunol 2020;11:573405.
[34] Tian J, Ashique AM, Weeks S, et al. ILT2 and ILT4 drive myeloid suppression via both overlapping and distinct mechanisms. Cancer Immunol Res 2024;12(5):592–613.
[35] Wang J, Shi Y, Gao Y, et al. Targeting macrophage-derived SPP1 enhances CD8 T cell infiltration via ROS-DNA fragment/cGAS-STING/STAT1-mediated CXCL9/10 in tumor microenvironment. J Immunother Cancer 2026;14(1).

Keywords: Hepatocellular carcinoma; Atezolizumab; Bevacizumab; immunotherapy; primary resistance; myeloid phenotype.
Received 4 September 2025; received in revised form 5 May 2026; accepted 21 May 2026; Available online xxx